UNIVERSITY OF WEST BOHEMIA

Applied and Computational Mechanics 3 (2009) 5–16

Applied and Computational Mechanics

Three-phase phononic materials

R. Cimrman[a,*], E. Rohan[a]

[a] *Department of Mechanics & New Technologies Research Centre, Faculty of Applied Sciences, University of West Bohemia, Univerzitní 22, 306 14 Plzeň, Czech Republic*

Received 29 September 2008; received in revised form 25 February 2009

Abstract

We consider a strongly heterogeneous material consisting of three phases: an elastic matrix, medium-size inclusions periodically embedded in the elastic matrix; these inclusions are constituted by small rigid inclusions coated by a very compliant material. The dependence on scale of elasticity coefficients of the deformable medium-size inclusions is treated in the context of linear elasticity by the homogenization procedure providing a limit model that inherently describes band gaps in acoustic wave propagation. The band gaps occur for certain intervals of long wavelengths for which a frequency-dependent "mass density" tensor is negative. We illustrate the theoretical results with numerical simulations.

Keywords: three-phase material, homogenization, rigid inclusion, acoustic band gaps

1. Introduction

We present an approach to modelling the phononic materials. These materials are similar to better known photonic crystals, cf. [4, 8, 13], but the main interest lies in modelling the propagation of elastic waves instead of light waves. Both the phononic and photonic materials exhibit forbidden frequency ranges of incident waves, for which the sound/light waves cannot propagate: the structure is blocked from free vibrations. In the context of sound wave propagation the forbidden frequency ranges are called *acoustic band gaps*. This wave dispersion feature has a lot of serious practical applications, such as acoustic wave guides, or silencers. Such smart materials are already being produced and their properties experimentally verified, cf. [11]; this raises the need for proper modelling tools able to predict their behaviour.

In this article we treat a strongly heterogeneous material consisting of three phases: an elastic matrix, medium-size inclusions periodically embedded in the elastic matrix; these inclusions are constituted by small rigid inclusions coated by a very compliant material (rubber, or epoxy resin). Considering the rigid inclusions is a new contribution and generalizes the two-phase material analyzed in [2, 3, 10]. The elasticity coefficients of the deformable medium-size inclusions depend on the scale. This is treated in the context of linear elasticity by the homogenization procedure providing a limit homogenized model that inherently describes band gaps in acoustic wave propagation.

The homogenization based prediction of the band gap distribution (i.e. analysis of the effective mass tensor eigenvalues) is relatively simple and effective in comparison with the "standard computational approach" based on a finite scale heterogeneous model, which requires to evaluate all the Brillouin zone for the dispersion diagram reconstruction; as the consequence, it

*Corresponding author. Tel.: +420 377 634 711, e-mail: cimrman3@ntc.zcu.cz.

leads to a killing complexity, namely when the inverse problem (optimal design) is considered. This is the main advantage of the homogenization based two-scale modeling. As an important restriction, this modeling approach is relevant for the long wave propagation, see [10].

We should point out that while band-gaps never occur in homogeneous or weakly heterogeneous materials, the "homogenized" material is rather a mathematical model of seemingly homogeneous material with "hidden" components — the underlying heterogeneous structure responsible for the dispersion is inherited by the model in terms of its effective parameters (the inertia mass and elasticity); this was discussed newly in [9], where a "generalized" Newton's second law was presented.

The model proposed in Section 3 is implemented in our open-source software SfePy, [5]. Numerical examples are presented in Section 5; mainly the influence of the rigid inclusion size on the band gap distribution is shown.

2. Problem setting

We consider a strongly heterogeneous material occupying an open bounded domain $\Omega \subset \mathbb{R}^3$ consisting of three phases, see Fig. 1. The first phase is an elastic matrix, the second phase corresponds to medium-size inclusions periodically embedded in the elastic matrix. These inclusions themselves are constituted by small rigid inclusions coated by a very compliant material (rubber). The rigid inclusions represent the third phase. The domain Ω is constituted as a periodic lattice structure generated by unit periodic reference cell $Y =]0,1[^3$ scaled by ε. The rigid inclusion $Y_3 \subset Y$ has the boundary Γ_3 and is coated by Y_2, so that $Y_2 \cap Y_3 = \emptyset$ and $\overline{(Y_2 \cup Y_3)} \subset Y$, $\overline{Y_2} \cap \overline{Y_3} = \Gamma_3$; the matrix part is $Y_1 = Y \setminus \overline{(Y_2 \cup Y_3)}$, see Fig. 2. We denote $Y_{2+3} = Y \setminus Y_1$.

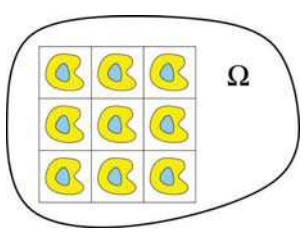

Fig. 1. Strongly heterogeneous material

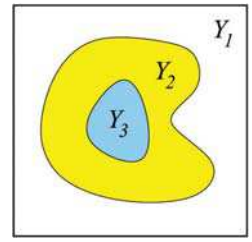

Fig. 2. Periodic reference cell

In Section 2.1 we define the three-phase strongly heterogeneous medium (SHM), then in Section 2.2 we recall the equations governing stationary waves in SHM developed in [10], and finally, in Section 3 we describe the resulting homogenized model, also based on results in [10].

2.1. Strongly heterogeneous material

The material properties, being attributed to material constituents of the three phases, vary periodically with position. Throughout the text all quantities varying with this microstructural periodicity are denoted with superscript $^\varepsilon$. Using the reference cell Y we generate the decomposition of Ω as follows

$$\Omega_2^\varepsilon = \bigcup_{k \in \mathbb{K}^\varepsilon} \varepsilon(Y_2 + k) \;, \text{ where } \mathbb{K}^\varepsilon = \{k \in \mathbb{Z} |\; \varepsilon(k + \overline{Y_2}) \subset \Omega\} \;,$$

$$\Omega_3^\varepsilon = \bigcup_{k \in \mathbb{K}^\varepsilon} \varepsilon(Y_3 + k) \;, \quad \Omega_1^\varepsilon = \Omega \setminus (\Omega_2^\varepsilon \cup \Omega_3^\varepsilon) \;,$$

so that $\overline{\Omega} = \overline{\Omega_1^\varepsilon \cup \Omega_2^\varepsilon \cup \Omega_3^\varepsilon}$.

Properties of a three dimensional body made of the elastic material are described by the elasticity tensor c^{ε}_{ijkl}, where $i, j, k, l = 1, 2, \ldots, 3$. As usual we assume both major and minor symmetries of c^{ε}_{ijkl} ($c^{\varepsilon}_{ijkl} = c^{\varepsilon}_{jikl} = c^{\varepsilon}_{klij}$).

The key assumption of the modelling is that *the material density* is comparable in subdomains $\Omega^{\varepsilon}_2 \cup \Omega^{\varepsilon}_3$ and Ω^{ε}_1, while the stiffness coefficients in the medium-size inclusions Ω^{ε}_2 are significantly smaller than in the matrix Ω^{ε}_1. The stiffness of the small inclusions Ω^{ε}_3 is much higher than in Ω^{ε}_2 so that it can be considered as rigid. In reality, stiffness of a material is corelated with its mass. Thus, because of small density of the material in Ω^{ε}_2, the role of Ω^{ε}_3 is an added mass so that the assumption of comparable densities in $\Omega^{\varepsilon}_2 \cup \Omega^{\varepsilon}_3$ and Ω^{ε}_1 is fulfilled. The *strong heterogeneity* is related to the geometrical scale of the underlying microstructure by coefficient ε^2, as follows:

$$\rho^{\varepsilon}(x) = \begin{cases} \rho^1 & \text{in } \Omega^{\varepsilon}_1, \\ \rho^2 & \text{in } \Omega^{\varepsilon}_2, \\ \rho^3 & \text{in } \Omega^{\varepsilon}_3, \end{cases} \qquad c^{\varepsilon}_{ijkl}(x) = \begin{cases} c^1_{ijkl} & \text{in } \Omega^{\varepsilon}_1, \\ \varepsilon^2 c^2_{ijkl} & \text{in } \Omega^{\varepsilon}_2, \\ (1/\varepsilon^2) c^3_{ijkl} & \text{in } \Omega^{\varepsilon}_3, \end{cases} \tag{1}$$

where $\rho^3 \gg \rho^2$. We shall consider positive densities: let $0 < \underline{\rho}, \overline{\rho} \in \mathbb{R}$, we assume $\underline{\rho} < \rho^{\varepsilon}(x) < \overline{\rho}$ a.e. in Ω. Further, we assume standard ellipticity and boundedness of the elastic coefficients: let S^+ be the set of all symmetric real second order tensors in $\mathbb{R}^3$, then $\forall e_{ij}, \hat{e}_{ij} \in S^+$, $\exists \underline{\mu}, \overline{\mu} > 0$ such that

$$\underline{\mu}\, e_{ij} e_{ij} \leq c^{\alpha}_{ijkl} e_{ij} e_{kl} \quad \text{and} \quad c^{\alpha}_{ijkl} e_{ij} \hat{e}_{kl} \leq \overline{\mu}\, e_{ij} \hat{e}_{ij} \ , \quad \alpha = 1, 2, 3 \ . \tag{2}$$

2.2. Modelling the stationary waves

We consider a stationary wave propagation in the SHM, see [10]. For simplicity we restrict the model to the description of clamped structures loaded by volume forces. Let us assume harmonic single-frequency volume forces,

$$\boldsymbol{F}(x, t) = \boldsymbol{f}(x) e^{\mathrm{i}\omega t} \ , \tag{3}$$

where $\boldsymbol{f} = (f_i), i = 1, 2, 3$ is the local amplitude and ω is the frequency. We consider a dispersive displacement field with the local magnitude $\boldsymbol{u}^{\varepsilon}$

$$\boldsymbol{U}^{\varepsilon}(x, \omega, t) = \boldsymbol{u}^{\varepsilon}(x, \omega) e^{\mathrm{i}\omega t} \ . \tag{4}$$

This allows us to study the steady periodic response of the medium, as characterized by the displacement field $\boldsymbol{u}^{\varepsilon}$ which satisfies the following boundary value problem:

$$\begin{aligned} -\omega^2 \rho^{\varepsilon} \boldsymbol{u}^{\varepsilon} - \mathrm{div} \boldsymbol{\sigma}^{\varepsilon} &= \boldsymbol{f} \quad \text{in } \Omega, \\ \boldsymbol{u}^{\varepsilon} &= 0 \quad \text{on } \partial\Omega, \end{aligned} \tag{5}$$

where the stress tensor $\boldsymbol{\sigma}^{\varepsilon} = (\sigma^{\varepsilon}_{ij})$ is expressed in terms of the linearized strain tensor $\boldsymbol{e}^{\varepsilon} = (e^{\varepsilon}_{ij})$ by the Hooke's law $\sigma^{\varepsilon}_{ij} = c^{\varepsilon}_{ijkl} e_{kl}(\boldsymbol{u}^{\varepsilon})$. The problem (5) can be formulated in the weak form as follows: Find $\boldsymbol{u}^{\varepsilon} \in \mathbf{H}^1_0(\Omega)$ such that

$$-\omega^2 \int_{\Omega} \rho^{\varepsilon} \boldsymbol{u}^{\varepsilon} \cdot \boldsymbol{v} + \int_{\Omega} c^{\varepsilon}_{ijkl} e_{kl}(\boldsymbol{u}^{\varepsilon}) e_{ij}(\boldsymbol{v}) = \int_{\Omega} \boldsymbol{f} \cdot \boldsymbol{v} \quad \text{for all } \boldsymbol{v} \in \mathbf{H}^1_0(\Omega) \ , \tag{6}$$

where $\mathbf{H}^1_0(\Omega)$ is the standard Sobolev space of vectorial functions with square integrable generalized derivatives and with vanishing trace on $\partial\Omega$, as required by $(5)_2$.

3. Homogenized model

We wish to associate the SHM model (6) with a homogeneous model relevant to the macroscopic scale. For this task *methods of homogenization* are widely accepted. Due to the *strong heterogeneity* in the elastic coefficients the homogenized model exhibits dispersive behaviour; this phenomenon cannot be observed when standard two-scale homogenization procedure is applied to a medium with scale-independent material parameters, as pointed out in [1]. In [3] the unfolding operator method of homogenization [6, 7] was applied with the strong heterogeneity assumption (1); it can be shown that $\boldsymbol{u}^\varepsilon \to \boldsymbol{u}$ as $\varepsilon \to 0$, where $\boldsymbol{u}$ is the "macroscopic" displacement field describing behaviour of the homogenized medium. Here we just record the resulting system of coupled equations which describe the structure behaviour at two scales, the "macroscopic" one and the "microscopic" one, since the theoretical considerations remain the same as in [10].

First we define the homogenized coefficients involved in the homogenized model of wave propagation. The "frequency-dependent coefficients" are determined just by material properties of the inclusion Y_{2+3} and by the material density ρ^1, whereas the elasticity coefficients are related exclusively to the matrix compartment Y_1.

Frequency-dependent homogenized coefficients involved in the macroscopic momentum equation are expressed in terms of eigenelements of the following spectral problem.

3.1. Spectral problem

Let us define a space of functions that describe *rigid body motions* (RBM) in Y_3 and are zero on the boundary of Y_{2+3}:

$$\boldsymbol{S}_0(\bar{y}, Y_3, Y_{2+3}) = \{\boldsymbol{v} \in \mathbf{H}^1_0(Y_{2+3}) \mid \exists(\bar{s}_{ij}, \bar{\boldsymbol{v}}) \ : \ v_i = \bar{v}_i + \bar{s_{ij}}(y_j - \bar{y}_j) \ , \ \forall y \in Y_3\} \ , \qquad (7)$$

where $(\bar{s}_{ij}, \bar{\boldsymbol{v}})$ is the spin–translation couple and $\bar{y}$ is the barycentre of Y_3. We shall employ the following notation:

$$a_{Y_m}(\boldsymbol{u}, \boldsymbol{v}) = \int_{Y_m} c^m_{ijkl} e^y_{kl}(\boldsymbol{u})\, e^y_{ij}(\boldsymbol{v}),$$
$$\varrho_{Y_m}(\boldsymbol{u}, \boldsymbol{v}) = \int_{Y_m} \rho^m \boldsymbol{u} \cdot \boldsymbol{v},$$

for $m = 2, 3$. The spectral problem for eigenelements $(\lambda^r, \boldsymbol{\varphi}^r)$, $\lambda^r \in \mathbb{R}$, $\boldsymbol{\varphi}^r \in \boldsymbol{S}_0(\bar{y}, Y_3, Y_{2+3})$, noting that $a_{Y_3}(\boldsymbol{\varphi}^r, \boldsymbol{v}) \equiv 0$ due to RBM constraint in Y_3, is:

$$a_{Y_2}(\boldsymbol{\varphi}^r, \boldsymbol{v}) = \lambda^r \left[\varrho_{Y_2}(\boldsymbol{\varphi}^r, \boldsymbol{v}) + \varrho_{Y_3}(\boldsymbol{\varphi}^r, \boldsymbol{v})\right] \ , \quad \forall \boldsymbol{v} \in \boldsymbol{S}_0(\bar{y}, Y_3, Y_{2+3}) \ , \qquad (8)$$

where

$$\varrho_{Y_2}(\boldsymbol{\varphi}^r, \boldsymbol{\varphi}^s) + \varrho_{Y_3}(\boldsymbol{\varphi}^r, \boldsymbol{\varphi}^s) = \delta_{rs} \ . \qquad (9)$$

It is easy to see that the orthogonality in (9) holds and $0 < \lambda^r \in \mathbb{R}$; indeed, $a_{Y_2}(\cdot, \cdot)$ is the elliptic bilinear form on $\mathbf{H}^1(Y)$. In the sequel we shall need the *eigenmomentum* $\boldsymbol{m}^r = (m^r_i)$,

$$\boldsymbol{m}^r = \int_{Y_2} \rho^2 \boldsymbol{\varphi}^r + \int_{Y_3} \rho^3 \boldsymbol{\varphi}^r. \qquad (10)$$

3.2. Homogenized coefficients

The homogenized coefficients can be computed in much the same way, as it was done for just two-phase composite, cf. [3, 10], when the role of Y_2 is substituted by the union Y_{2+3}. We recover the following tensors, all depending on ω^2:

- mass tensor $\boldsymbol{M}^* = (M^*_{ij})$

$$M^*_{ij}(\omega^2) = \frac{1}{|Y|}\int_Y \rho\delta_{ij} - \frac{1}{|Y|}\sum_{r\geq 1}\frac{\omega^2}{\omega^2-\lambda^r} m_i^r m_j^r \; ; \tag{11}$$

- applied load tensor $\boldsymbol{B}^* = (B^*_{ij})$

$$B^*_{ij}(\omega^2) = \delta_{ij} - \frac{1}{|Y|}\sum_{r\geq 1}\frac{\omega^2}{\omega^2-\lambda^r} m_i^r \int_{Y_2}\varphi_j^r \; . \tag{12}$$

The elasticity coefficients are related to the perforated matrix domain, thus being independent of the inclusions material:

$$C^*_{ijkl} = \frac{1}{|Y|}\int_{Y_1} c^1_{pqrs} e^y_{rs}(\boldsymbol{w}^{kl} + \boldsymbol{\Pi}^{kl}) e_{pq}(\boldsymbol{w}^{ij} + \boldsymbol{\Pi}^{ij}) \; , \tag{13}$$

where $\boldsymbol{\Pi}^{kl} = (\Pi^{kl}_i) = (y_l\delta_{ik})$ and $\boldsymbol{w}^{kl} \in \mathbf{H}^1_\#(Y_1)$ are the corrector functions satisfying

$$\int_{Y_1} c^1_{pqrs} e^y_{rs}(\boldsymbol{w}^{kl} + \boldsymbol{\Pi}^{kl}) e^y_{pq}(\boldsymbol{v}) = 0 \quad \forall \boldsymbol{v} \in \mathbf{H}^1_\#(Y_1) \; . \tag{14}$$

Above $\mathbf{H}^1_\#(Y_1)$ is the restriction of $\mathbf{H}^1(Y_1)$ to the Y-periodic functions (periodicity w.r.t. the homologous points on the opposite edges of ∂Y).

3.3. Macromodel

The *global equation* — the macromodel — involves the homogenized coefficients. We find $\boldsymbol{u} \in \mathbf{H}^1_0(\Omega)$ such that

$$-\omega^2 \int_\Omega (\boldsymbol{M}^*(\omega^2)\cdot\boldsymbol{u})\cdot\boldsymbol{v} + \int_\Omega C^*_{ijkl} e_{kl}(\boldsymbol{u})\, e_{ij}(\boldsymbol{v}) = \int_\Omega (\boldsymbol{B}^*(\omega^2)\cdot\boldsymbol{f})\cdot\boldsymbol{v} \; , \quad \forall \boldsymbol{v} \in \mathbf{H}^1_0(\Omega) \, . \tag{15}$$

Heterogeneous structures with finite scale of heterogeneities exhibit the frequency *band gaps* for certain frequency bands. As the main advantage of this homogenized model, by analyzing the dependence $\omega \to \boldsymbol{M}^*(\omega)$ one can determine distribution of the band gaps with significantly less effort than in case of analyzing them in the standard way, see e.g. [12]. In [10] an exhaustive description of band gaps computations is given, some of which is summarized in Section 4.

4. Band gaps

In the context of our homogenization-based modelling of phononic materials, the band gaps are frequency intervals for which the propagation of waves in the structure is disabled or restricted in the polarization.

The band gaps can be classified w.r.t. the polarization of waves which cannot propagate. Given a frequency ω, there are three cases to be distinguished according to the signs of eigenvalues $\gamma^r(\omega)$, $r = 1, 2, 3$ (in 3D), which determine the "positivity, or negativity" of the mass:

1. **propagation zone** — all eigenvalues of $M^*_{ij}(\omega)$ are positive: then homogenized model (15) admits wave propagation without any restriction of the wave polarization;

2. **strong band gap** – all eigenvalues of $M^*_{ij}(\omega)$ are negative: then homogenized model (15) does *not* admit any wave propagation;

3. **weak band gap** — tensor $M^*_{ij}(\omega)$ is indefinite, i.e. there is at least one negative and one positive eigenvalue: then propagation is possible only for waves polarized in a manifold determined by eigenvectors associated with positive eigenvalues. In this case the notion of wave propagation has a local character, since the "desired wave polarization" may depend on the local position in Ω.

We denote the smallest and the highest eigenvalues of $M^*_{ij}(\omega)$ by $\gamma^{\triangledown}(\omega)$ and $\gamma^{\triangle}(\omega)$, respectively.

4.1. Computing the band gaps

Distribution of the band gaps is based on analyzing the eigenvalues of tensor $\boldsymbol{M}^*(\omega)$ which is a nonlinear function (11) of ω. Therefore, in general, it can be done numerically using a finite element (FE) approximation of eigenvalue problem (8), see Section 4.2. Thus we obtain a finite number n_h of the approximated eigenvalues and their associated eigenfunctions $(\lambda^r, \boldsymbol{\phi}^r)$, $r = 1, \ldots, n_h$; here n_h is the number of free displacement degrees of freedom (dofs) for a given FE mesh.

From the theoretical analysis of a similar homogenized "phononic" problem, which was done for rectangular domain Y_2 and the Laplace operator it follows that the homogenized coefficient analogous to the mass tensor (11) is expressed in terms of series containing integrals of the type (10), which vanish "exactly" for some modes. Due to this let us define the *eigenmode cut-off threshold* $c > 0$ and introduce the *set of non-zero modes*

$$\mathcal{I}_h(c) \equiv \{1 \leq k \leq n_h | \quad |\boldsymbol{m}^k_h| > c\}, \tag{16}$$

where $\boldsymbol{m}^k_h$ is evaluated according to (10), i.e.

$$\boldsymbol{m}^k_h = \int_{Y_{2,h}} \rho^2 \boldsymbol{\phi}^r + \int_{Y_{3,h}} \rho^3 \boldsymbol{\phi}^r \ . \tag{17}$$

Then, denoting the averaged density $\bar{\rho}$, the homogenized mass tensor is computed by

$$M^*_{ij}(\omega) = \delta_{ij}\bar{\rho} - \frac{\omega^2}{|Y|} \sum_{k \in \mathcal{I}_h(c)} \frac{1}{\omega^2 - \lambda^k} m^k_{i,h} m^k_{j,h} \ , \quad i,j = 1,2,3 \ . \tag{18}$$

4.2. Discrete eigenvalue problem: enforcing RBM constraints

The FE-discretized counterpart of (8) is to seek $(\lambda^r, \boldsymbol{\phi}^r)$, $\lambda^r \in \mathbb{R}$, $\boldsymbol{\phi}^r \in \boldsymbol{S}_{h0}(\bar{y}, Y_3, Y_{2+3})$ and

$$\mathbf{v}^T \mathbf{A} \boldsymbol{\phi}^r = \lambda^r \mathbf{v}^T \mathbf{M} \boldsymbol{\phi}^r \ , \quad \forall \mathbf{v} \in \boldsymbol{S}_{h0}(\bar{y}, Y_3, Y_{2+3}) \ , \tag{19}$$

where $r = 1, \ldots, n_h$ with n_h the number of free displacement dofs and $\boldsymbol{S}_{h0}$ is just a finite element approximation to $\boldsymbol{S}_0$. Below we show how to construct such a solution that obeys the RBM constraint.

Let us assume to have the standard matrices $\bar{\mathbf{A}}$, $\bar{\mathbf{M}}$, corresponding to FE-discretized operators $a_{Y_2}(\boldsymbol{u}, \boldsymbol{v})$ and $\varrho_{Y_{2+3}}(\boldsymbol{u}, \boldsymbol{v})$, such that the fixed zero displacements on Γ_{2+3} are already eliminated. Correspondingly, let us define also $\bar{\mathbf{v}}$, $\bar{\boldsymbol{\phi}}$. To enforce the RBM constraint the following splitting can be used:

$$\bar{\mathbf{v}} = \begin{bmatrix} \mathbf{v}_f \\ \mathbf{v}_r \end{bmatrix}, \quad \bar{\mathbf{A}} = \begin{bmatrix} \mathbf{A}_{ff} & \mathbf{A}_{fr} \\ \mathbf{A}_{rf} & \mathbf{A}_{rr} \end{bmatrix}, \tag{20}$$

where the suffix $_f$ relates to the free dofs and $_r$ to the RBM-constrained dofs. Analogously we split also $\bar{\boldsymbol{\phi}}$, $\bar{\mathbf{M}}$. The constrained dofs in a point y can be expressed as

$$\mathbf{v}_r(y) = \left[\begin{array}{ccc|ccc} 0 & y_3 & -y_2 & 1 & 0 & 0 \\ -y_3 & 0 & y_1 & 0 & 1 & 0 \\ y_2 & -y_1 & 0 & 0 & 0 & 1 \end{array}\right] \begin{bmatrix} \boldsymbol{\theta} \\ \mathbf{v}_0 \end{bmatrix} \equiv \mathbf{R}(y)\boldsymbol{\theta} + \mathbf{I}\mathbf{v}_0 \equiv \mathbf{T}(y)\mathbf{s}\,, \tag{21}$$

where $\mathbf{s} = \begin{bmatrix} \boldsymbol{\theta} & \mathbf{v}_0 \end{bmatrix}^T$, $\mathbf{R}(y)\boldsymbol{\theta}$ is a linearized rotation of y w.r.t. 0 by a spin $\boldsymbol{\theta}$ and $\mathbf{v}_0$ is a translation. In 2D, $\mathbf{R}(y)\theta \equiv \begin{bmatrix} -y_2 & y_1 \end{bmatrix}^T \theta$ and θ is a scalar. Repeating this for each FE mesh node, we can write $\mathbf{v}_r = \mathbf{T}\mathbf{s}$, $\boldsymbol{\phi}_r = \mathbf{T}\mathbf{r}$. The eigenvalue problem (19) can thus be written as

$$\begin{bmatrix} \mathbf{v}_f^T & \mathbf{s}^T\mathbf{T}^T \end{bmatrix} \begin{bmatrix} \mathbf{A}_{ff} & \mathbf{A}_{fr} \\ \mathbf{A}_{rf} & \mathbf{A}_{rr} \end{bmatrix} \begin{bmatrix} \boldsymbol{\phi}_f \\ \mathbf{T}\mathbf{r} \end{bmatrix} = \lambda^r \begin{bmatrix} \mathbf{v}_f^T & \mathbf{s}^T\mathbf{T}^T \end{bmatrix} \begin{bmatrix} \mathbf{M}_{ff} & \mathbf{M}_{fr} \\ \mathbf{M}_{rf} & \mathbf{M}_{rr} \end{bmatrix} \begin{bmatrix} \boldsymbol{\phi}_f \\ \mathbf{T}\mathbf{r} \end{bmatrix}. \tag{22}$$

The multiplications by the constraint matrix $\mathbf{T}$ can now be carried out to arrive at (19) with

$$\mathbf{v} = \begin{bmatrix} \mathbf{v}_f \\ \mathbf{s} \end{bmatrix}, \; \boldsymbol{\phi} = \begin{bmatrix} \boldsymbol{\phi}_f \\ \mathbf{r} \end{bmatrix}, \; \mathbf{A} = \begin{bmatrix} \mathbf{A}_{ff} & \mathbf{A}_{fr}\mathbf{T} \\ \mathbf{T}^T\mathbf{A}_{rf} & \mathbf{T}^T\mathbf{A}_{rr}\mathbf{T} \end{bmatrix}, \; \mathbf{M} = \begin{bmatrix} \mathbf{M}_{ff} & \mathbf{M}_{fr}\mathbf{T} \\ \mathbf{T}^T\mathbf{M}_{rf} & \mathbf{T}^T\mathbf{M}_{rr}\mathbf{T} \end{bmatrix}. \tag{23}$$

5. Numerical examples

The numerical examples presented below were computed using our finite element code SfePy, [5], that is freely available at http://sfepy.org. Changes in the band gap distribution due to

1. varying the cut-off threshold c,
2. symmetry / nonsymmetry of the rigid inclusion Y_3 placement in Y_{2+3}, and thus also the underlying FE mesh,
3. varying the size of the rigid inclusion Y_3

are shown. In all the examples the domain $Y \in \mathbb{R}^2$ was $[-1, 1]^2$, and Y_{2+3} was a circle centered at $[0, 0]^T$ with radius 0.8, see Fig. 3. Material properties were defined as follows:

material	subdomain	Lamé coefficients [10^{10} Pa]	density [10^4 kg/m^3]
aluminium	Y_1	$\lambda^1 = 5.898$, $\mu^1 = 2.681$	$\rho^1 = 0.2799$
epoxy	Y_2	$\lambda^2 = 0.1798$, $\mu^2 = 0.148$	$\rho^2 = 0.1142$
lead	Y_3	$\lambda^3 = 4.074$, $\mu^3 = 0.5556$	$\rho^3 = 1.1340$

The above materials/properties were chosen considering which materials had been typically used for production of phononic devices. We remark that in our computation the third material (lead) is considered as rigid.

The FE-discretized eigenvalue problem (8) was solved in Y_{2+3} with the clamped boundary ∂Y_{2+3} ($= \partial\bar{Y}_2 \cap \partial\bar{Y}_3$) and with the RBM constraint in Y_3, see Section 4.2. The computed eigenvalues and eigenvectors $(\lambda^r, \boldsymbol{\phi}^r)$ were then used to construct the mass tensor $\boldsymbol{M}^*(\omega)$ given by (18) and to evaluate the band gap distribution for a given frequency range according to the signs of the eigenvalues of $\boldsymbol{M}^*(\omega)$, see Section 4. The eigenmomentum cut-off threshold c was chosen as

$$c = 0.1 \max_{k=1\ldots n_h} |\boldsymbol{m}_h^k| \,,$$

with exception of Section 5.1, where it was the subject of a parametric study. Similarly, the radius of the rigid inclusion was $r(Y_3) = 0.45$ with exception of Section 5.3.

Note: When plotting the eigenvalues $\gamma^{\triangledown}(\omega)$, $\gamma^{\triangle}(\omega)$ we transform them by $\arctan$ function to zoom to the interesting behaviour near zero.

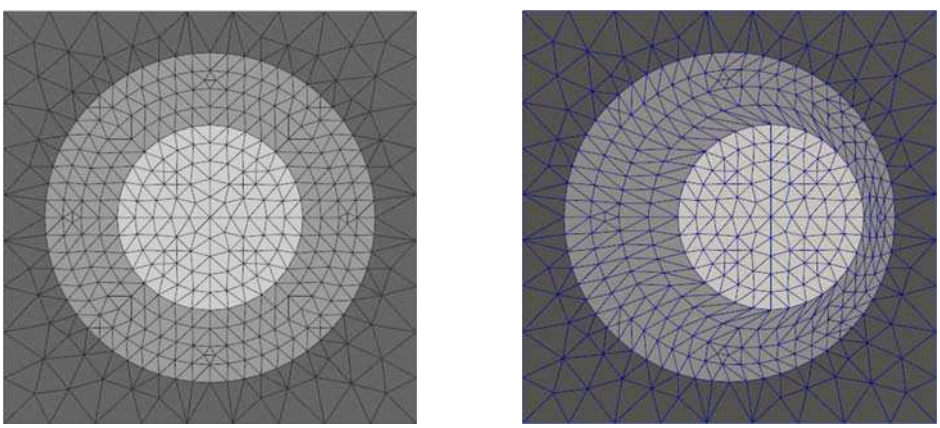

Fig. 3. FE meshes; left: symmetric Y_{2+3}, right: shifted Y_3. The eigenvalue problem is computed in the circular domain Y_{2+3} only

5.1. Cut-off threshold

For $f \in [0, 25]$ kHz we have conducted a parametric study by setting $c = 10^q \max_{k=1\ldots n_h} |\boldsymbol{m}_h^k|$ for $q = -3 + 0.5j$, $j = 0, \ldots, 6$ using the mesh with unsymmetric Y_3 placement, see Fig. 3 (right). In this case we had $n_h = 307$ eigenmomenta out of which the following numbers were under threshold:

j	0	1	2	3	4	5	6
masked	28	104	222	285	301	305	306

The resulting band gaps and $\gamma^{\triangledown}(\omega)$, $\gamma^{\triangledown}(\omega)$ plots are shown in Fig. 4 for $j = 0, 4, 6$. It can be seen that for $j = 4$, i.e. $c = 0.1 \max_{k=1\ldots n_h} |\boldsymbol{m}_h^k|$ the band gaps are almost the same as for $j = 0$, but the spurious oscillations in $\gamma^{\triangledown}(\omega)$, $\gamma^{\triangledown}(\omega)$ are removed. These results support our choice of c in the other examples.

5.2. Inclusion symmetry

Here we numerically verify the theoretical result derived in [10] saying that the weak band gaps cannot appear if the inclusion is symmetric. This behaviour can be observed for the three-phase

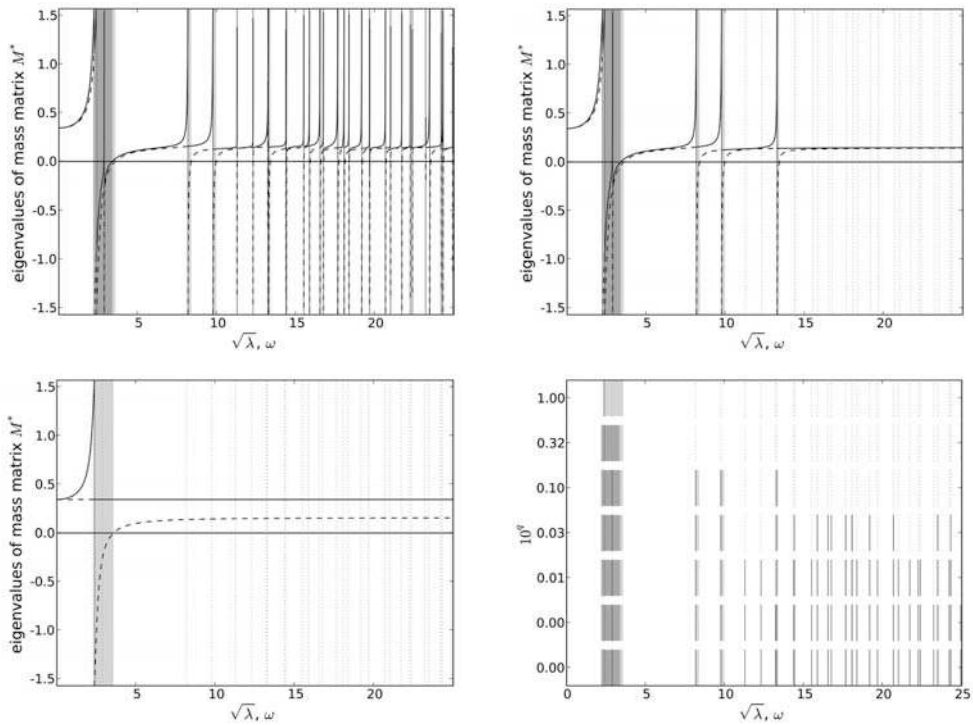

Fig. 4. Band gap distribution; top left: $j = 0$, top right: $j = 5$, bottom left: $j = 10$, bottom right: overview for all $q = -3 + 0.5j$, $j = 0, \ldots, 6$; $\arctan \gamma^{\triangledown}(\omega)$: dashed lines, $\arctan \gamma^{\triangle}(\omega)$: solid lines, strong band gaps: gray, weak band gaps: light gray, propagation zone: white, resonance frequencies: solid vertical lines, resonance frequencies masked by c: dotted vertical lines

material too. For $f \in [0, 15]$ kHz a sequence of simulations was performed, starting with a perfectly symmetric shape, see Fig. 3 (left). The rigid inclusion Y_3 was then shifted in steps of 0.02 along the x axis up to the final position (shift = 0.2) depicted in Fig. 3 (right).

As predicted, no weak band gaps appear in Fig. 5 (top left), corresponding to the symmetric shape, as opposed to Fig. 5 (top right), corresponding to the most shifted Y_3. All the cases, including the intermediate Y_3 positions, are summarized in Fig. 5 (bottom).

5.3. Size of the rigid inclusion

The sizes of the rigid inclusion $r(Y_3)$ were varied for both the symmetric and unsymmetric Y_3 placements, see Fig. 6; the results are summarized in Fig. 7 for $f \in [0, 25]$ kHz. These results suggest that increasing the inclusion size causes broadening of the band gap corresponding to the lowest eigen-frequency computed by (19), and also growth of the separation between the first and the subsequent band gaps. The latter observation is more pronounced in the symmetric case.

6. Conclusion

The purpose of the paper was to present some aspects of modelling of the wave propagation in the strongly heterogeneous elastic medium using the homogenized model that was adapted

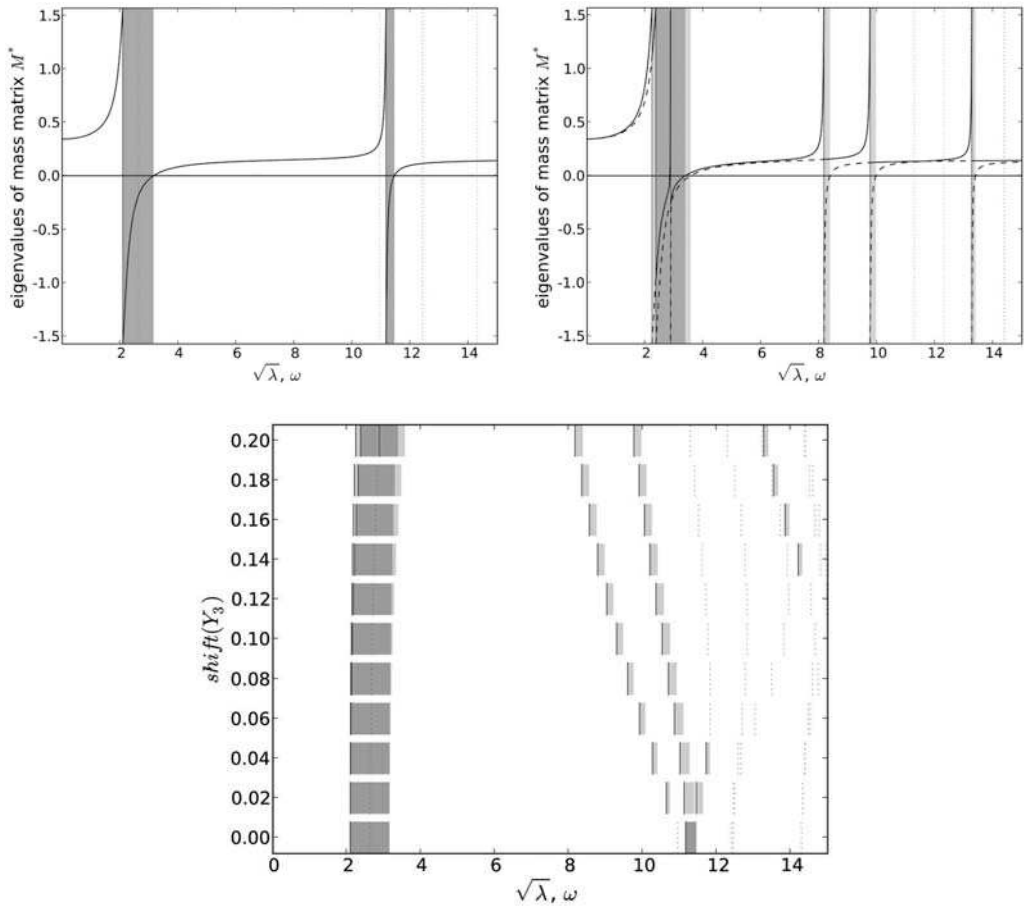

Fig. 5. Band gap distribution on two FE meshes; top left: symmetric, bottom: summary for all Y_3 positions, top right: max. shift; $\arctan \gamma^{\triangledown}(\omega)$: dashed lines, $\arctan \gamma^{\triangle}(\omega)$: solid lines, strong band gaps: gray, weak band gaps: light gray, propagation zone: white, resonance frequencies: solid vertical lines, resonance frequencies masked by c: dotted vertical lines

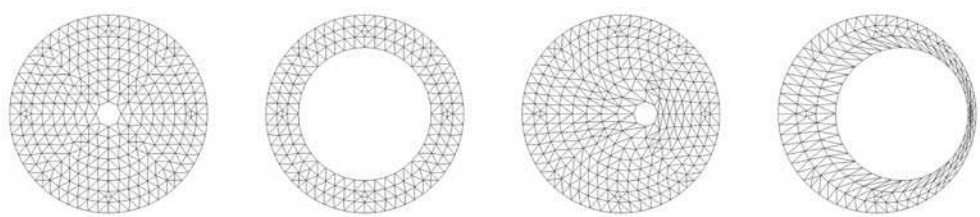

Fig. 6. Examples of meshes of Y_2 when varying $r(Y_3)$. The domains Y_1, Y_3 are not shown to stress the fact that no finite element analysis is needed there. From left to right: symmetric, $r = 0.1$; $r = 0.54$; unsymmetric, $r = 0.1$; $r = 0.54$

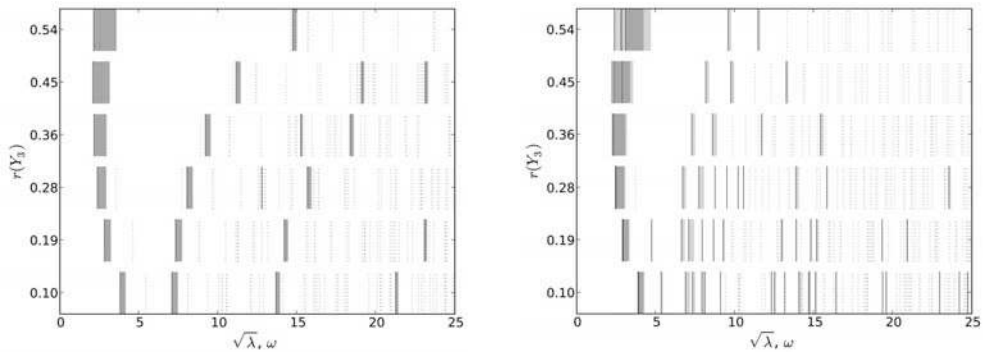

Fig. 7. Band gap distribution for varying $r(Y_3)$; left: symmetric, right: shifted Y_3 position; strong band gaps: gray, weak band gaps: light gray, propagation zone: white, resonance frequencies: solid vertical lines, resonance frequencies masked by c: dotted vertical lines

from [10] to a three-phase phononic material (elastic matrix, inclusions made of small rigid bodies coated by a very compliant material). Introducing the *rigid inclusions* into the model is the main new result of the paper. It was motivated by the need to satisfy the key assumption of the modelling: that the material density has to be comparable in both the matrix and the inclusions, while the stiffness coefficients in the inclusions should be significantly smaller than in the matrix. The rigid inclusions, thus, represent an added mass in the soft (and light) medium-size inclusions.

The principal ingredient of the homogenization procedure is the scale dependence of the elastic coefficients in the mutually disconnected inclusions — this leads to acoustic band gaps due to the *negative effective mass* phenomenon appearing in the upscaled model.

The main advantage of the homogenization based two-scale modeling lies in the fact, that the homogenization based prediction of the band gap distribution for stationary or long guided waves is relatively simple and effective, cf. [10], in comparison with the "standard computational approach" based on a finite scale heterogeneous model, which requires to evaluate all the Brillouin zone for the dispersion diagram reconstruction; as the consequence, it leads to a killing complexity. Moreover, in [10] a correspondence between our band gap diagrams and the classical dispersion diagrams was discussed.

We demonstrated in several numerical examples that these band gaps can be effectively computed. We studied how the prediction of the band gap distribution changes when varying the rigid inclusion size and other parameters.

Acknowledgements

The work has been supported by the Czech Science Foundation, grant GAČR 101/07/1471, and the Czech Government project 1M06031.

References

[1] J. L. Auriault and G. Bonnet. Dynamique des composites elastiques periodiques. *Arch. Mech.*, (37):269–284, 1985.

[2] A. Ávila, G. Griso, and B. Miara. Bandes phononiques interdites en élasticité linéarisée. *C. R. Acad. Sci. Paris*, I(340):933–938, 2005.

[3] A. Ávila, G. Griso, B. Miara, and E. Rohan. Multi-scale modelling of elastic waves — theoretical justification and numerical simulation of band gaps. *Multiscale Modeling and Simulation, SIAM*, 2007.

[4] G. Bouchitté and D. Felbacq. Homogenization near resonances and artificial magnetism from dielectrics. *C. R. Acad. Sci. Paris*, Ser. I(339):377–382, 2004.

[5] R. Cimrman et al. SfePy home page. http://sfepy.kme.zcu.cz, http://sfepy.org, 2008.

[6] D. Cioranescu, A. Damlamian, and G. Griso. Periodic unfolding and homogenization. *C. R. Acad. Sci. Paris*, I(335):99–104, 2002.

[7] A. Damlamian. An elementary introduction to periodic unfolding. *GAKUTO International series Math. Sci. Appl.*, 24:119–136, 2005. Multi scale problems and Asymptotic Analysis.

[8] D. Felbacq and G. Bouchitté. Theory of mesoscopic magnetism in photonic crystals. *Phys. Rev. Lett.*, 94:183–902, 2005.

[9] G. W. Milton and J. R. Willis. On modifications of newton's second law and linear continuum elastodynamics. *Proc. R. Soc. A*, (483):855–880, 2007.

[10] E. Rohan, B. Miara, and F. Seifrt. Numerical simulation of acoustic band gaps in homogenized elastic composites. *accepted to Int. J. Eng. Sci.*, 2009. doi:10.1016/j.ijengsci.2008.12.003.

[11] Ping Sheng, X. X. Zhang, Z. Liu, and Chan C. T. Locally resonant sonic materials. *Physica B: Condensed Matter*, 338(1–4):201–205, 2003.

[12] O. Sigmund and J. S. Jensen. Systematic design of phononic band-gap materials and structures by topology optimization. *Phil. Trans. R. Soc. London*, A(361):1 001–1 019, 2003.

[13] E. Yablonovitch. Photonic band-gap crystals. *J. Phys. Condens. Mat.*, 5:2 443–2 460, 1993.